Ultramicroscopy 22 (1987) 89–102
North-Holland, Amsterdam

LOCAL BONDING AND ELECTRONIC STRUCTURE OBTAINED FROM ELECTRON ENERGY LOSS SCATTERING

P.E. BATSON, K.L. KAVANAGH *, C.Y. WONG and J.M. WOODALL

IBM Thomas J. Watson Research Center, Yorktown Heights, New York 10598, USA

Received 26 september 1986; presented at Conference April 1986

Preliminary results using the new high resolution Wien filter spectrometer coupled to the scanning transmission electron microscope show that it is now possible to investigate atomic bonding, and both filled and empty electronic states in inhomogeneous materials with a 1 nm spatial resolution. We show three examples: (1) identification of a 5 nm layer of Si_2N_2O at a Si/Si_3N_4 interface using core-loss near-edge fine structure, (2) observation of effects due to changes in the conduction band density of states due to Si–Si bond disorder at the Si/SiO_2 interface, and (3) identification of a filled defect electronic state associated with a single misfit dislocation at a GaAs/GaInAs interface.

1. Introduction

Electron energy-loss scattering (EELS) has been pursued for several years now as a possible technique for the quantitative determination of the composition of materials [1]. Unfortunately, the most direct method for accomplishing this – direct measurement of the scattering intensity and subsequent comparison to calculated cross-sections to obtain the absolute amount of material present [2] – suffers from several annoying problems. Experimental difficulties include the accurate determination of: angular collection conditions, which change significantly as a function of energy loss [3]; the shape of the background intensity, which is crucial for estimation of the scattering intensity in each core loss [4]; multiple inelastic scattering, which complicates interpretation [5] and increases the amount of intensity data needed to get an accurate core loss area [6]. Further, the theoretical determinations of scattering cross-sections are still crude, yielding, at best, accuracies of $\pm 10\%$ [7].

This work investigates the feasibility of alternative techniques based on a detailed analysis of the shapes of energy-loss features with a high enough energy resolution to identify contributions arising from electronic structure. Within 10 eV of a core ionization edge, these contributions have been called Energy-Loss Near-Edge Structure (ELNES) [8], and have been identified as giving information specific to bonding symmetry in various compounds [9]. The results of the present work indicate that in some instances ELNES structure may be dominated by a subset of the local anti-bonding orbitals, producing similar structure in different atomic environments. Thus "family resemblances" noted earlier by others [9] might be explained.

The detailed shape within 1 eV of the core edge yields information about the empty states of the material [10]. In addition, the precise location of the core ionization onset can be influenced by charge transfer [11], core excitonic binding [12], and shifts in the Fermi level [13]. Thus, Si $L_{2,3}$ spectra contain structure related to conduction band states at Γ, Δ and L in the Brillouin zone [14]. We report here changes in this structure near the Si/SiO_2 interface which are interpreted as results of Si–Si bonding disorder.

In the very low energy-loss region (less than 2 eV), we observe energy-loss scattering resulting from direct inter-band excitations in semiconductors and insulators. This scattering is sensitive to

* Department of Materials Science and Engineering, Cornell University, Ithaca, New York 14853, USA.

0304-3991/87/$03.50 © Elsevier Science Publishers B.V.
(North-Holland Physics Publishing Division)

changes in both the conduction and valence bands. It is possible to measure the bulk band-gap in small regions of a heterogeneous sample. In addition, modifications of the gap due to isolated structural defects are visible. We show experimental results which identify a filled defect electronic state associated with a single misfit dislocation at the GaAs/GaInAs interface. A simple inelastic scattering cross-section analysis indicates that the scattering associated with an isolated defect of this type is unexpectedly strong.

2. Experiment

This work was carried out with a Wien filter electron spectrometer [15] coupled to the VG Microscopes, HB501 STEM. A typical energy resolution of 0.35 eV was maintained with a collection semi-angle of 12.5 mrad at 100 keV for energy losses up to about 300 eV. The collection semi-angle was increased to 25 mrad for collection of higher losses, giving a resolution of approximately 0.5–0.6 eV. The energy-loss position accuracy for the instrument is ± 50 meV over a time period of as much as an hour. However, in some of the results at high energy loss, the statistical accuracy of these data does not allow that accuracy to be used. We estimate that the absolute energy measurements in this work are accurate to ± 0.05 eV for the Si $L_{2,3}$ edges, ± 0.3 eV for the N K edges and ± 1.0 eV for the O K edges examined in this work. The data for the spectra below were acquired for times of 5–20 s per point, leading to total acquisition times of 10 min to over an hour for a spectrum requiring many points. These long acquisition times are a result of the low STEM beam current (0.5–2 nA), and the high energy resolution, requiring small energy selecting slits (about 50 meV). For the high spatial resolution experiments, radiation damage becomes a concern, leading to limits on the total possible collection time and resulting in data of limited statistical accuracy. In the future, we hope that parallel detection systems will reduce this problem. Presently, we are adding a parallel diode array to this system which, together with some other modifications, should increase the collection efficiency by about $\times 10^3$. It should then be possible to greatly enhance the interpretability of the data presented below.

We did not attempt to quantify effects due to radiation damage in these experiments. However, we did verify that the results for the bulk materials obtained with a very large probe (> 1 μm) were similar to those obtained with the 1 nm probe. It was possible, under conditions of a very small probe (< 1 nm), to observe time-dependent changes in the energy-loss structure that presumably were a result of radiation damage. We report here only those results that we believe are free of this problem.

3. ELNES structure of Si-derived compounds

We begin by describing results for various Si-derived compounds. These show interesting correlations of energy-loss structure for similar atomic environments. These similarities allow us to make a tentative identification of the composition of a 5 nm layer of unknown material occurring at a Si/Si_3N_4 interface.

The specimens consisted of various amorphous and crystalline preparations of the above mentioned compounds. Two forms of SiO were investigated – the bulk commercial material and a thin evaporated film. These gave identical results. Amorphous Si_3N_4 from CVD preparation was used. Si_2N_2O was in crystalline, powder form. Spectra were obtained from thin areas on the edges of small crystallites of unknown orientation. Various forms of SiO_2 – CVD, high temperature thermal, α quartz, and native – were investigated. All gave similar results on the scale of ± 0.2 eV. Detailed differences on a scale smaller than this will be discussed elsewhere [16]. The heterogeneous sample consisted of crystalline Si with its surface prepared by a reactive ion etch (RIE) and subsequently covered by CVD deposited Si_3N_4 [17]. The $Si–Si_3N_4$ interface was revealed in cross-section by standard techniques of cutting and ion beam milling. TEM inspection of this interface revealed a 8 nm thick layer of unknown composition as shown in fig. 1.

In all of these compounds, Si is tetrahedrally

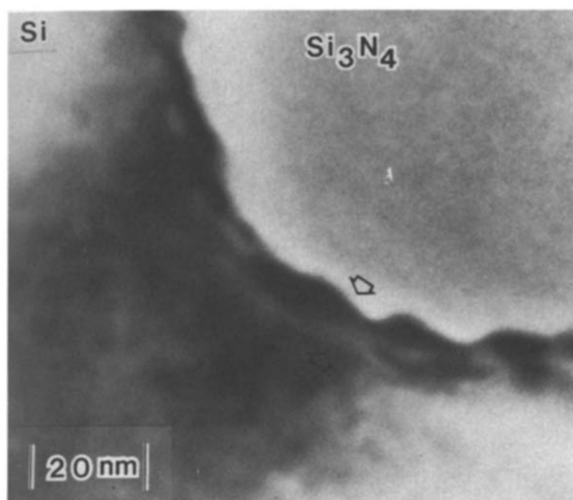

Fig. 1. Bright field image of the Si–Si_3N_4 interface showing a 8 nm thick layer of unknown material at the interface.

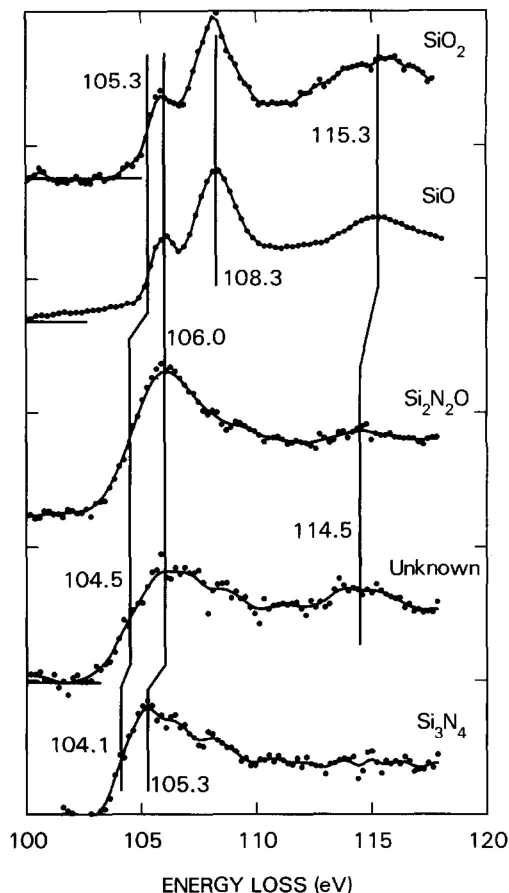

Fig. 2. Si $L_{2,3}$ intensity data obtained for various Si-derived compounds compared to those obtained for the unknown layer. The unknown intensity was obtained from the analysis described with fig. 5.

coordinated. In SiO_2, each Si is surrounded by four O, while in SiO, each Si has, on average, two Si and two O neighbors. In Si_2N_2O, Si and N form a roughly planar network with O forming bridges between Si atoms in different networks [18], and with N always coordinated with three Si neighbors. Si_3N_4 is comprised of a complex interconnection of locally planar networks with Si coordinated tetrahedrally by N, and N coordinated trigonally by Si [19].

4. Results and discussion

Fig. 2 shows the results for the Si $L_{2,3}$ core excitation for the various compounds. In each case we have subtracted a background intensity of the form ΔE^{-r} which has been fitted over an energy range of about 10 eV before the edge. This procedure has been discussed in detail by Egerton [4]. In this work, this background estimation need not be particularly accurate because we are not trying to measure absolute scattering intensities. Relatively large errors in the background can be tolerated because they will not grossly alter the positions of the near edge structure. This is especially true over the rather limited energy range that the present results cover. Also, for this analysis, plasmon multiple scattering effects can be neglected because these will not produce additional structure below 15 eV beyond the edge. If the probed volume is thick, these measured intensities will be reduced by multiple scattering to higher energies. But the detailed structure of these results will not be altered.

In this series of results, the core loss onset is shifted quite a long way from the measured bulk Si L_3 onset at 99.8 eV [20]. This shift is largely due to the shift in the conduction band density of states resulting from the opening of an insulating bandgap. Further effects result from a chemical shift of the core state itself as Si becomes increas-

ingly oxidized. However, we shall suggest below that this effect may not be apparent in the energy-loss results for transitions to highly localized final states. Finally, the large upward shift in energy of the conduction band in the ground state of the insulating material is partially compensated by a downwards shift in the localized final states for the excited state of the crystal – the core exciton [12]. Due to the presence of these many and complicated processes, it is difficult to ascribe the small shifts in fig. 2 to particular physical effects. However, at this point, it is interesting to notice that the observed structures for SiO_2 and SiO are nearly identical even though the oxidation state of the Si should be quite different in the two cases. It is well known from XPS work for instance, that the Si core level shifts by 2 eV in going from Si^{2+} (Si coordinated with 2 O and 2 Si) to Si^{4+} (Si coordinated with 4 O [11]).

The detailed shapes of these core losses – the number and strength of ELNES peaks – are extremely difficult to predict, although some progress has been made recently [8,10,21,22]. This difficulty is largely due to the core excitonic effects. Since the energy-loss scattering produces an excited state of the material that includes a hole in the core state, the final electronic density of states is distorted by the nearby presence of this positive charge. This process can shift peak positions, change the relative intensity of ELNES structure, and even introduce new structure [12,21,23]. This effect is strongest for materials having a small dielectric constant, such as insulators, weaker in semiconductors, and even less important in metals. This is due to the reduction of effective charge of the core hole by valence and conduction electronic screening. Since the excitonic distortion of the final states is localized near the core hole, we expect that materials which have strong excitonic behavior will give spectra which are not sensitive to long-range periodicities. For instance, SiO_2 has a strong excitonic shift of ~ 2.5 eV [23] for the L_{23} excitation. Thus crystalline and amorphous SiO_2 show nearly identical spectra. We therefore suspect that the Si $L_{2,3}$ spectra in that case may be associated with final states comprised of antibonding orbitals associated with the SiO_4 tetrahedral unit. This notion seems to be supported by calculations [22].

As fig. 2 shows, however, very similar $L_{2,3}$ spectra are obtained for both SiO_2 and SiO, where each Si has on average only two O neighbors. We conclude that the characteristic spectral structure must arise from a smaller sub-unit of the SiO_4 tetrahedron. This conclusion is supported by more experimental evidence, shown below, but theoretical calculations will be necessary to confirm it.

Si_3N_4, on the other hand, shows little structure above its onset peak at 105.3 eV. We have noticed evidence for structure near 108 eV, which is confirmed by others [24], but it is not clearly present in fig. 2. The Si_2N_2O absorption lies intermediate in position between Si_3N_4 and SiO_2 with peaks at 106.0 eV and at 114.5 eV, similar to SiO_2, but with an overall shape which is more consistent with Si_3N_4.

Since N and O are similar atoms (for instance charge transfer to Si has been calculated to be

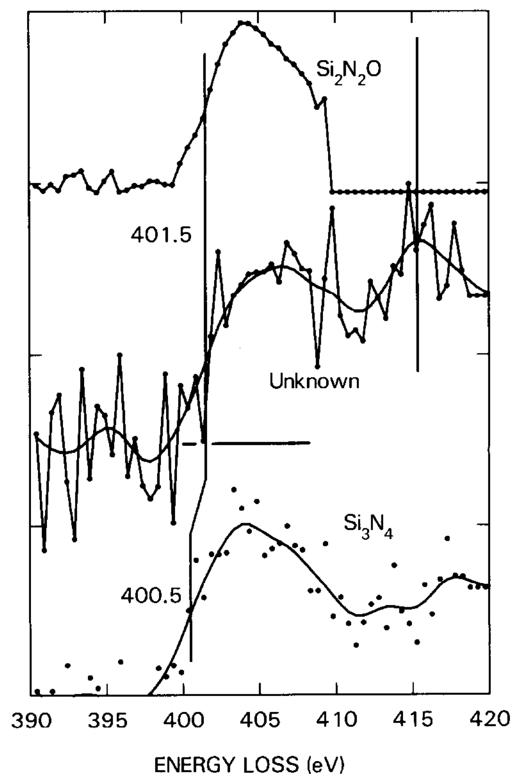

Fig. 3. N K intensity data. The small shift in energy between Si_2N_2O and Si_3N_4 is statistically significant and probably related to charge transfer effects.

1.99e for Si_2N_2O and 2.1e for Si_3N_4 [18]) and since all these materials have similar band gaps [19,18,23], we expect to observe similar excitonic effects in the $L_{2,3}$ spectra. Therefore, we expect to see similar features in the spectra, provided that the final states are similar. Thus, the similarity in the shape of the $L_{2,3}$ onset (within 2 eV of the edge) in Si_3N_4 and Si_2N_2O suggests that this intensity is dominated by the N environment, while the peak at 114.5 eV may be O related (perhaps an anti-bonding orbital formed at the Si–O–Si bridge). Further, the disappearance of the peak at 108.3 eV and the weakening of the onset intensity in going from SiO_2 and SiO to Si_2N_2O may signal that these features depend on orbitals related to the O–Si–O bonding configuration. This structure remains intact on going from SiO_2 to SiO, but is destroyed on going from SiO to Si_2N_2O. All of this, of course, is highly speculative

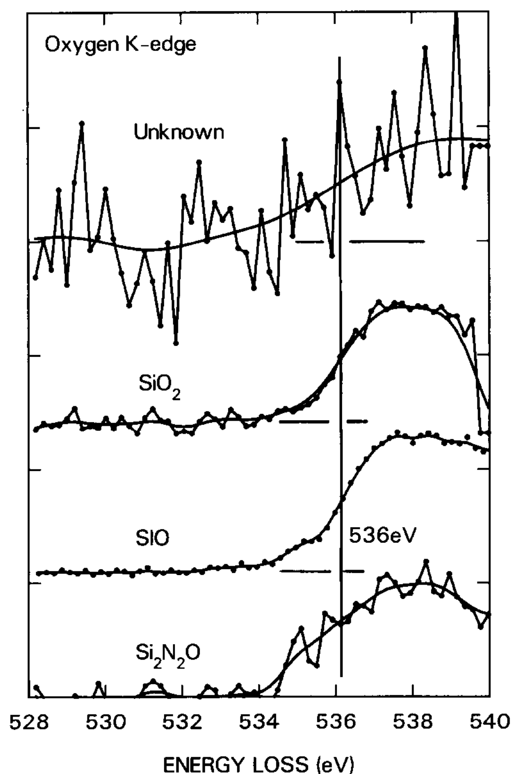

Fig. 4. O K intensity data. These data are remarkably similar although statistical accuracy limits position comparisons to ±1 eV.

and will require theoretical work to support.

Turning to the nitrogen K edge in fig. 3, we notice a small shift from the free nitrogen ionization core position at 399 eV. The similarity of the shapes and positions of these results for Si_3N_4 and Si_2N_2O supports the above discussion which notes that the nitrogen environments are similar in the two compounds.

In fig. 4, we show results for the O K excitation. We see a remarkable similarity in the edge positions, with the onset being located at 536 eV, fully 4 eV above the ESCA-obtained binding energy of oxygen at 532 eV. There do appear to be differences in the shapes of these edges in going from the oxides to the oxy-nitride. However, the present statistical accuracy probably is not good enough for positive comparisons to be made. The large upwards shift in energy from the free atom value is reminiscent of the upwards shift in the Si $L_{2,3}$ edge from that obtained for bulk Si. In the case of SiO_2 it is well known that the first Si conduction band states have both s and p character derived from the oxygen [23]. We also know that the oxygen near-neighbor environment is similar for SiO, SiO_2, and Si_2N_2O [18]. We thus speculate from the similarity of the spectra in fig. 4 that the O K edge structure is determined by the local environment of the oxygen (the Si–O–Si bond), which is similar for these compounds.

We mentioned above that the chemical shift as measured by XPS did not seem to be present in the Si $L_{2,3}$ edges in the oxides. This also appears to be the case for the O K excitation. We have argued above that the final states for these losses are probably highly localized due to excitonic effects. We suspect, therefore, that charge transfer effects are minimized for these losses because both the core level and the final state levels are shifted in energy by similar amounts. Notice that this argument applies only if the final state is highly localized about the site of the charge transfer. Thus, the charge state of the Si in SiO_2 and SiO is irrelevant because the final Si–O–Si derived states are suspected to be localized. A detailed examination [16] of the region between 100 and 105 eV in SiO reveals structure which is possibly derived from Si hybrids anti-bonding with O, but with larger Si influence than is present in SiO_2. This is

suggested by a calculation of the Si-centered local density of states at a $Si-SiO_2$ interface [25], where the local atomic configuration is similar to SiO. That calculation shows final state intensity within the SiO_2 gap, and so could mitigate the appearance of intensity below the $L_{2,3}$ onset in the SiO spectra. However, little can be said about possible excitonic effects for this possibility.

5. The unknown material

These results were all obtained from bulk samples with little constraint imposed by contamination, specimen drift, radiation damage, or other problems related to the task of obtaining analytical information from small areas. The problem outlined in fig. 1 requires that we obtain reasonable quality data from a small area of a truly heterogeneous structure. How well can we do at this task?

Close examination of fig. 1 reveals that the interface between the Si and Si_3N_4 is not smooth, consisting of 3–5 nm high "hillocks". These are likely similar to those observed by Scanning Tunneling Microscopy [26] on ion beam damaged Si surface. Since the present Si surface was processed via Reactive Ion Etching (RIE), this similarity is reasonable. Thus, even for probe positions exactly in the center of the 8 nm layer, we expect to see some bulk Si and bulk Si_3N_4 contributions. Fig. 5 shows the result for the Si $L_{2,3}$ edge from the unknown layer. Clearly some bulk Si scattering at 99.8 eV is present. Probably some bulk Si_3N_4 scattering is present also. We have fitted the scattering between 99 and 101 eV with the bulk Si scattering and have subtracted to obtain the middle curve of fig. 5. Based on the relative magnitude of the fitted Si intensity to that obtained in the bulk Si immediately adjacent to the layer, we estimate that 12% of the thickness of the probed volume in the layer was actually bulk Si, probably located at high points of the "hillocks". We next scaled the measured bulk Si_3N_4 intensity to 12% thickness as well and subtracted to obtain the curve labeled "Unknown" in the figure. This treatment obviously assumes that we managed to hit the precise center of the unknown layer, and

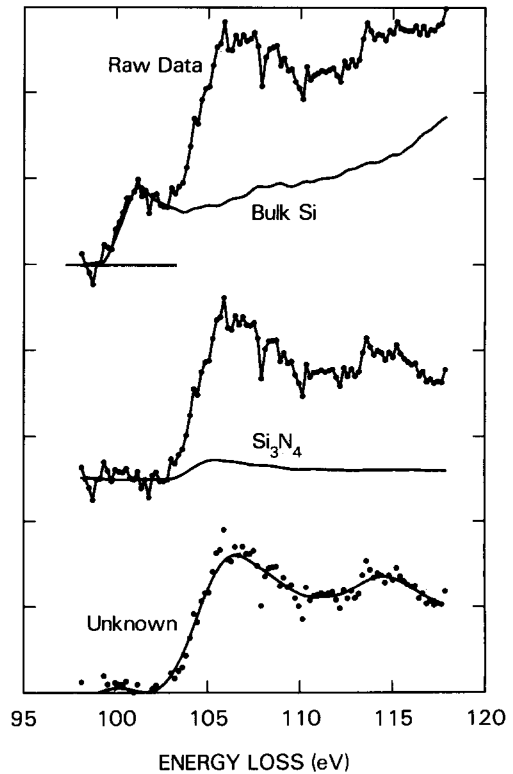

Fig. 5. Processing of the raw data from the unknown interface layer to eliminate bulk Si and Si_3N_4 signal due to contribution from "hillocks" which reach into the layer from either side of the interface layer.

that the roughness of the layer was controlled completely by the RIE process. A gross error in this estimate will shift the final edge position by as much as 1 eV, so this uncertainty should be remembered in the discussion below. However, a variation of the bulk Si_3N_4 contribution to the data from 12% to 80% did not change the position or the relative prominence of the 114.5 eV peak. Returning now to figs. 2, 3, and 4, it becomes apparent that a very good match can be made between the unknown material and Si_2N_2O. It is also apparent that reliance on any one core edge for our analytical determination would lead to confusion. On the other hand, we can say from a simple observation of the oxygen edge that (a) oxygen is present and (b) it is likely bonded to Si in a way similar to oxygen in SiO_2. Then, observation of a Si $L_{2,3}$ edge that does not resemble the

SiO_2 result implies strongly that there is at least one other constituent present in the compound.

6. Bond disorder at interfaces

The next example concerns the extreme near edge structure on the Si L_3 edge near the crystalline/amorphous interface between Si and SiO_2. The specimen consisted of 8 nm of thermally oxidized SiO_2 on a [111] oriented Si substrate with a 20 nm thick polycrystalline Si over-layer. The specimen was subsequently annealed at 900 ° C for 10 min. The sample was cut along the [110] Si plane for cross-section preparation by chemical and ion-beam thinning. Fig. 6 shows a bright field STEM image of the layer taken at 2×10^6 magnification. Bulk Si with the [110] orientation lies to the left of the SiO_2 layer, while polycrystalline Si lies to the right. The focus in this image was adjusted to maximize contrast for displaying morphology. The focus for EELS analysis was adjusted for a spot size of 0.8 nm.

In fig. 7, we show a result for bulk crystalline Si

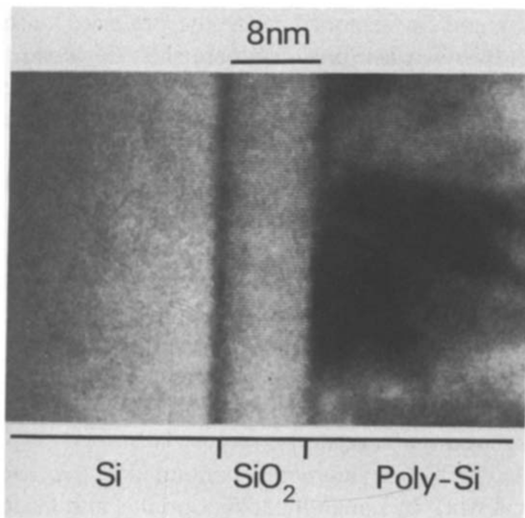

Fig. 6. Bright field image of the Si–SiO_2–poly-Si structure viewed in cross-section. The thickness of the SiO_2 is about 8 nm. This image was obtained under conditions which maximize contrast, leading to a spreading of the observed Si–SiO_2 interface image. EELS data were obtained under conditions to minimize the electron probe size.

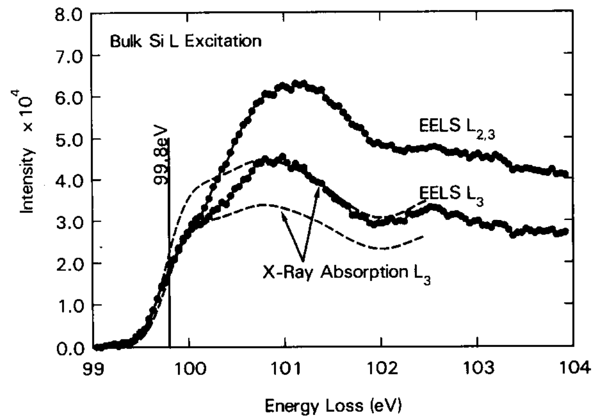

Fig. 7. A comparison of the EELS $L_{2,3}$ and L_3 bulk Si results with the results from X-ray absorption measurements. For the comparison, the X-ray results have been broadened by a 0.35 eV wide resolution function. The X-ray results are plotted with two gain factors to highlight (1) the very good energy alignment at 99.8 eV and (2) the enhancement of scattering to the conduction band minimum at Δ_1 at the expense of that to L_1 and Γ_{15}.

with a [110] direction oriented parallel to the electron beam. Each energy-loss point resulted from ~ 8 s of counting time during a total acquisition time of ~ 800 s. We have fitted and subtracted a background of the form ΔE^{-r} to eliminate multiple electronic scattering from lower energies [4]. The Si $L_{2,3}$ excitation onset occurs at 99.8 eV for final states at the conduction band minimum (Δ_1 in the Brillouin zone), with post edge structure corresponding to final states at L_1 and Γ_{15}. We have extracted the L_3 scattering assuming a spin–orbit splitting of 0.6 eV and a statistical weighting of 2 : 1 for the L_3 and L_2 contributions. This analysis is not strictly necessary for the present experiment, however it does allow a cleaner identification of final states, and therefore a more confident comparison of the EELS result with other techniques. We have compared the resulting L_3 intensity with the X-ray absorption results of Brown and Rustgi [14] derived in a similar way. We have broadened their data by convolution with a 0.35 eV wide Gaussian distribution for comparison. We have plotted the X-ray data with an intensity normalization at 100 eV to emphasize the energy alignment, and at 101 eV to point out that the major difference between

the two results appears to involve the relative amount of scattering to Δ_1 compared to the scattering involving Γ and L. We conclude that the EELS edge onset position agrees with the X-ray absorption result with an accuracy of ± 50 meV. We speculate that the different intensity of excitations reflects differences between the X-ray absorption matrix element which includes all possible vertical transitions, and EELS which required a momentum transfer largely within a plane perpendicular to the incident beam direction [27]. In passing, it is interesting to note that an excitonic interaction does exist for this edge, but is weak enough that it does not strongly shift the positions of the various final state contributions relative to each other [14].

In fig. 8, we show L_3 intensities obtained from two regions: (a) 2 nm into the bulk and (b) on the $Si-SiO_2$ interface. The position accuracy perpendicular to the boundary was ± 0.2 nm. The total integration time was ~ 2 s per point. The two spectra were processed as described above, and then normalized at 101 eV. The measured intensity at the boundary was about 13% of the intensity measured 2 nm into the bulk, with the two backgrounds appearing similar. We know from the discussion above that Si partially coordinated

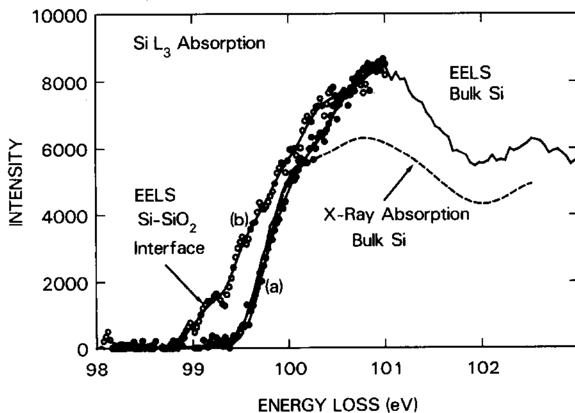

Fig. 8. Detailed comparison of the L_3 edge profiles from fig. 7 (dashed lines) with results obtained (a) 2 nm into Si from the $Si-SiO_2$ interface and (b) on the interface. The EELS spectra are normalized in the region 100.8 to 101 eV. A clear shift of order 0.3 eV appears on the scattering to Δ while a smaller effect of order 0.25 eV occurs for scattering to L_1.

by O produces an $L_{2,3}$ intensity largely above 104 eV. Therefore, the intensity recorded here is probably only produced by $Si-Si_4$ units, that is, only by Si fully coordinated by other Si. Since the density of these units at the interface is probably less than 25% of that in the bulk (one for every four interface Si atoms), the measured intensity is not unreasonably small. For the 0.8 nm probe, a position error of 0.2 nm could produce a large deviation from this density at the 0.2–0.5 nm wide interface. Each of these spectra were obtained by summation of three separate acquisitions at slightly different locations in the direction parallel to the boundary. The two results are compared with the better statistical results of fig. 2 above. We see a clear agreement with bulk Si for the position 2 nm away from the interface. For the position on the interface we see a significant shift downwards in energy by 0.2–0.3 eV. Scattering to both Δ_1 and L_1 show similar shifts. Inelastic scattering 2 nm into the oxide shows the expected shift of the L edge to 105.5 eV as shown above.

The observation of a shift downwards in energy is puzzling because XPS data show large upward shifts for increasing oxidation of Si in SiO [11]. Therefore, it seems unlikely that a core chemical shift could be responsible for the observed onset shift downwards. Some excitonic shift downwards may be expected since the normally strong dielectric screening of the bulk Si [14] may be reduced at the interface [28]. A surface band bending of 0.3 eV has been observed in amorphous Si [29] but we expect to have equal shifting on all electronic and core states, leading to no shift in the spectra. This results because band bending is an electrostatic effect, caused by the redistribution of charge carriers over a relatively large distance. Thus the energies of all bands are shifted equally by the extra background potential introduced by the charge redistribution.

A possible explanation is contained in the theoretical work of Laughlin, Joannopoulos and Chadi [25]. They have used a cluster-Bethe-lattice method to model the $Si-SiO_2$ interface. This method uses molecules which are representative of the local environment and which are embedded in a solid by attaching Bethe lattices to the dangling bonds of the molecules. The method is highly successful

in reproducing major features in both the valence and conduction bands of both Si and SiO_2. Using these ideas they concluded that (a) the ideal Si–SiO_2 interface is expected to show no new electronic structure, (b) a dangling bond at the interface will produce a strong midgap state and (c) bond disorder – both stretching and bending – produces additional local density of states near the top of the valence band and near the bottom of the conduction band [25]. The present results, therefore, cannot be explained by an ideal interface. Strong empty midgap states would not produce the observed shift either, since they should produce well separated structure ~ 0.5 eV below the $L_{2,3}$ onset. It should be emphasized however that the present results do not rule out the existence of midgap states because the statistical accuracy of the data in the 99.4–99.5 eV energy range is not adequate at the present time. Midgap states have been observed in $C-V$ and DLTS measurements of unannealed p-type MOS capacitors [30], but these were observed to disappear with mild annealing (450 °C). Since the present structures were annealed at 900 °C, we therefore do not expect a large midgap state density.

The most likely explanation for the present results is bond disorder. This was investigated further by Laughlin et al. [31] using the methods described above. They found that ±30° distortions of the Si–Si bond produced enhancements and small downward shifts of the local conduction band of states near the Si atom. In extreme cases, this effect may pull down a discrete state our of the conduction band. We believe therefore that the present experimental results support the view that Si–Si bonds near the well annealed Si–SiO_2 interface are subject to some bending or stretching.

7. Conclusions regarding core excitations

We have shown that there is a wealth of information available within the first few eV of the onset of typical core edges in Si derived compounds. This can be used for simple "fingerprint" analysis of unknown stoichiometries, and it may also be used for estimates of local atomic environments even in the presence of strong excitonic and chemical shifts. We suggest that, at least in these types of materials, the detailed shapes of the near edge structure are strongly related to the local bonding environment of the atoms. Thus the "family resemblance" of core losses has a relatively simple explanation. This interpretation further explains nicely the strong resemblances in these results in the absence of similar site symmetries. Finally, this information appears to be obtainable from the small areas of relevance to defect and interface related materials science. Future work in this area should include detailed studies of interfaces which have been well characterized by high resolution TEM. This kind of a study would allow an evaluation of the spatial localization of the energy-loss scattering. The results above indicate that a fairly high spatial resolution is obtainable in the STEM experiment for core excitations. Results described below indicate that this is true also for single particle transitions in the very low energy-loss region. Systematic experiments are needed to verify these possibilities.

8. The low energy-loss region

In semiconductors and insulators, we expect to observe energy loss due to direct single particle excitations across the bandgap. Until now, these processes have been difficult to observe due to their relatively small scattering intensity in the region dominated by the unscattered beam. The scattering cross-section per atom for fast electrons for a uniform medium of dielectric constant ϵ is given by [27]

$$\frac{\partial\sigma}{\partial E}=\frac{2}{\pi n a_0 E_0}\ln\left(\frac{\theta_c}{\theta_E}\right)\operatorname{Im}\left(\frac{-1}{\epsilon(E)}\right), \quad (1)$$

where eq. (1) is for a material with atomic density n, E_0 is the incident electron energy, a_0 is the Bohr radius, θ_c is the maximum scattering angle, and θ_E is related to the energy-loss in the usual way [27]. We use the atomic density, rather than the usual density of valence electrons, to obtain a cross-section per atom for comparison with the atomic core ionization calculation below. For the

bulk interband absorption in GaAs, we have estimated ϵ from the optical absorption data [32,33], finding the real part $\epsilon_1 = 11.2$ and the imaginary part $\epsilon_2 = 0.6$ at $E = 1.5$ eV. We estimate θ_c from the combined momentum width of the valence and conduction bands contributing to the near edge absorption. Eq. (1) gives $\partial\sigma/\partial E = 0.84 \times 10^{-22}$ cm^2 eV^{-1} atom^{-1}. This produces a scattering probability $P(E)\mathrm{d}E = 0.7 \times 10^{-5}$ into 0.1 eV wide slits for 200 nm of GaAs. Even with the nominal 0.30 eV wide intensity distribution from a cold field emission source, the incident beam intensity at 1.5 eV energy loss is as high as 10^{-5} of the intensity at 0 eV [34]. Therefore, without the aid of a monochromation system, it is necessary to separate the inter-band inelastic scattering from the incident beam intensity by subtraction. It is important for the success of this subtraction that the spectrometer have sufficient energy resolution to accurately define the shape of the field emission profile.

In fig. 9, we show an example of direct interband scattering GaAs. We have plotted the intensity on a log plot to emphasize the exponential behavior of the field emission profile due to electron emission from well below the Fermi level in the tip. The profile is compared with the total profile obtained in transmission through the GaAs to highlight the need for an adequate background subtraction procedure. In the inset in fig. 9, we show the difference between the two curves on a linear plot, labeled for cross-section. We show also in the inset results for a simple joint density of states model for transitions between two parabolic bands parameterized by effective masses m_h and m_c and separated by a gap E_g:

$$\left(\frac{m_c m_h}{m_c + m_h}\right)^{3/2} (E - E_g)^{1/2}. \tag{2}$$

This result is normalized for a best fit to the experimental data and convoluted with a resolution of 0.35 eV. A good fit is obtained for $E_g = 1.42$ eV, precisely the expected bulk value. A comparison of the measured interband intensity with the total intensity under the zero loss peak gives a measured cross-section $\partial\sigma/\partial E = 1.4 \times 10^{-22}$ cm^2 eV^{-1} atom^{-1}. The main uncertainty in this value derives from the thickness which was not measured, but which we estimate to have been be-

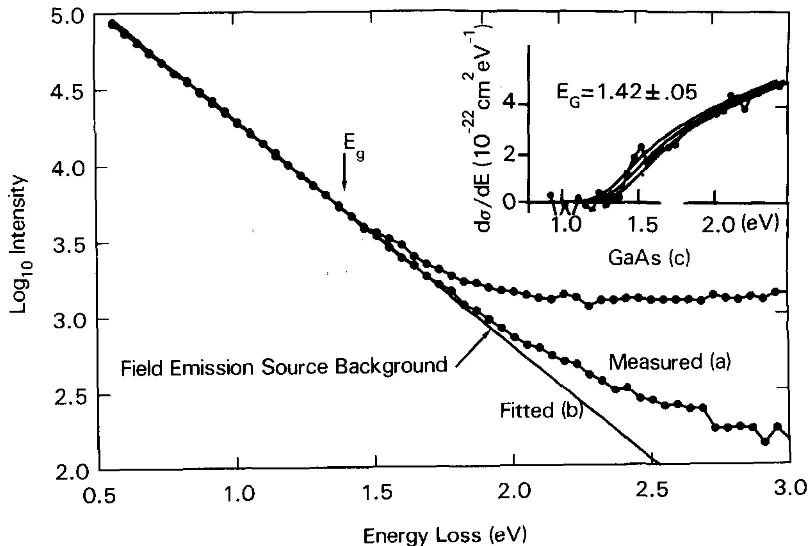

Fig. 9. Measured data for the field emission distribution (a) compared with the GaAs scattering (c). The extrapolated background (b) differs from the measured background only above 1.7 eV energy loss. The inset shows the difference between GaAs and the fitted background, labeled to show the differential scattering cross-section. The solid lines in the inset show the result of a parabolic band model with a 1.42 eV gap.

tween 200 and 400 nm. This thickness is larger than we normally use because GaAs is a relatively weak scatterer in the low energy-loss region, with $\mathrm{Im}(-1/\epsilon)$ being about half as big as for Si.

We expect that structural defects will affect the bandstructure in a small local volume in ways that may be observable. For instance, we noted above that it is fairly well accepted that dangling bonds will produce sharp electronic states deep within the gap [31]. Further, less radical deviations from ideal bonding (e.g. bond bending) can modify the band edges – even splitting off discrete states from the bands in extreme cases. The cross-section for scattering from a localized state will depend strongly on its physical size through the requirement for a reasonable overlap between the initial (localized) state and the final (presumably delocalized) state. We can estimate the size of a general defect state if we model it as a hydrogen atom with a small binding energy. We know that the effective core radius for the ground state of a Bohr atom with a binding energy E can be estimated,

$$r_c \sim a_0 E^{-1/2}. \tag{3}$$

This gives $r_c = 1.8$ Å for $E = 1$ eV. This value is very large with respect to all naturally occurring core radii, and results from a partial dielectric screening of the Bohr nucleus charge, parameterized by the specification of a binding energy. Thus, we expect a fairly large overlap between the core state and final electronic state wavefunctions, leading to a reasonably large inelastic scattering cross-section.

The cross-section for this process can be written in the Born approximation [35],

$$\frac{\partial\sigma}{\partial E} = \frac{4\pi e^4}{\epsilon_1^2 E_0} \ln\left(\frac{\theta_c}{\theta_E}\right) \frac{1}{E} \frac{\partial f}{\partial E}. \tag{4}$$

Eq. (4) is the result for an atomic core to continuum excitation characterized by a binding energy E and a generalized oscillator strength (GOS) $\partial f/\partial E$, embedded within a medium having a dielectric constant ϵ. The inclusion of $\mathrm{Re}(\epsilon) = \epsilon_1$ in this manner results from an evaluation of $\mathrm{Im}(-1/\epsilon)$ when the core ionization contribution to ϵ is larger than $\mathrm{Im}(\epsilon) = \epsilon_2$ for the bulk, but smaller than ϵ_1. In that case, ϵ_1 is dominated by the bulk medium, and ϵ_2 is dominated by the defect. In effect, the bulk medium screens the dielectric response of the defect, reducing the probability of scattering from what it would be in a vacuum. We estimate the GOS to be equal to that for ionization of hydrogen [35], noting that this number is between 0.01 and 0.2 eV^{-1} for most ionization processes and is not strongly atom dependent. Then, eq. (4) gives $\partial\sigma/\partial E = 0.6 \times 10^{-20}\,\mathrm{cm}^2\,\mathrm{eV}^{-1}\,\mathrm{state}^{-1}$ for the defect state scattering, almost 100 times larger than the bulk interband cross-section. The most likely physical reason for this result is due to the extremely small JDOS for direct interband transitions at Γ in GaAs. A comparison of the results of eq. (1) above for direct bulk scattering at Γ with defect scattering to a continuum, shows a disparity of about $\times 85$ in favor of the defect scattering [36].

In fig. 10, we show a STEM bright field image of a cross-section of a $\mathrm{GaAs/Ga_{0.85}In_{0.15}As}$ interface. A single $\frac{1}{2}a\langle 110\rangle$ type misfit dislocation is seen end-on in the center of the photo. Details of specimen preparation are described elsewhere [36,37]. Briefly, this sample was prepared by Molecular Beam Epitaxy techniques with a Si doping of about 2×10^{18} to produce n-type elec-

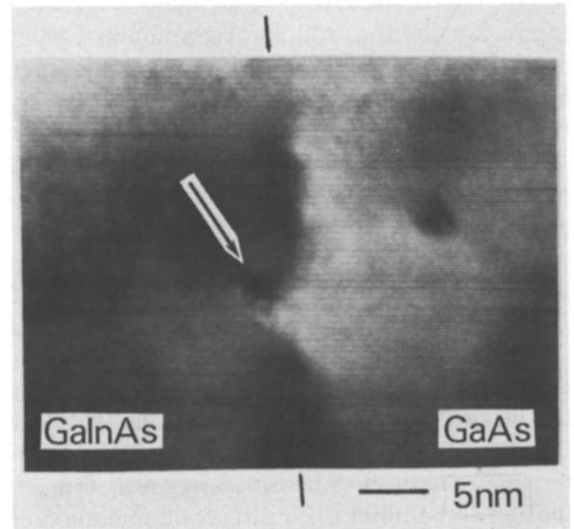

Fig. 10. Bright field image of the GaAs–GaInAs interface in the cross-section view specimen. A misfit dislocation is indicated by the arrow.

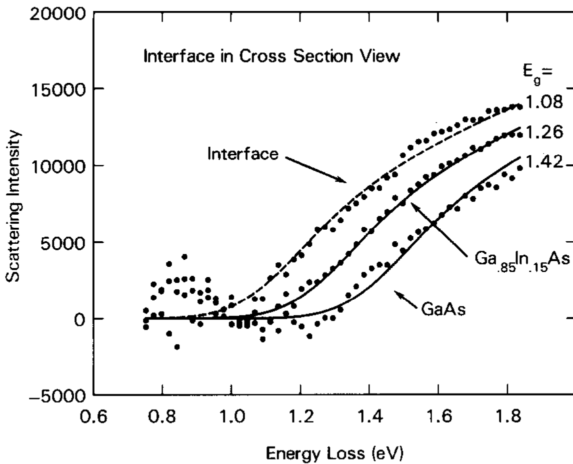

Fig. 11. Inelastic scattering after removal of the background intensity for GaAs, GaInAs, and the end-on dislocation shown in fig. 10. Model calculations for different bandgaps are included for comparison. Scatter in the data below 0.8 eV results from inaccurate subtraction of the large field emission background.

trical behavior. Deep level electronic states in this system are likely to be occupied, possibly pinning the Fermi level in a local region, to produce a Schottky barrier [37]. Fig. 11 shows the EELS absorption result for an area in the GaAs, in the GaInAs and near the misfit dislocation shown in fig. 10. We see the 1.42 eV gap in GaAs, a 1.26 eV gap in the GaInAs, and an absorption at 1.08 eV near the dislocation. The GaInAs result agrees nicely with a linear combination of the GaAs and InAs (0.36 eV [38]) values for a 15% In alloy.

We can deduce a defect electronic level energy position by considering the relationship of the defect bandstructure with the bandstructure of the solid. From the arguments above, we have suggested that the defect state will be localized. Therefore, we expect in reciprocal space a relatively flat band extending throughout the Brillouin zone. Thus, vertical electronic transitions from this band will be possible throughout the GaAs Brillouin Zone. Direct interband transitions near the threshold in the bulk occur only near Γ due to the narrow width of the maxima and minima there (~ 0.05 Å^{-1} at 1.5 eV). Therefore it is likely that the final states for the defect scattering may be different from those for the bulk scattering. Inspection of the conduction bands [39] for GaAs shows high densities of states 1.9 eV above the valence band at X (zone boundary in the 100 direction) and at 1.8 eV at L (zone boundary in the 111 direction). These are probably lowered slightly (of order 0.04 eV) by In alloying at the interface. Evaluation of eq. (2) above using $m_{\text{defect}} \sim \infty$ with effective masses appropriate to these indirect minima shows that practically all of the observed scattering will result from the final states at 1.76–1.86 eV above the valence band. Thus we locate the defect state at 1.08 eV below this point or 0.7 ± 0.05 eV above the top of the valence band. It is interesting, but by no means conclusive, that this position is consistent with that expected for a dangling bond [25,31].

These results were obtained with a 1–1.5 nm probe from regions separated by several tens of nanometers. Thus spatial localization in this low energy-loss region has not been tested. The rough comparison of the magnitude of dislocation scattering relative to the bulk, however, suggests that only the dislocations within the probed volume contribute to the observed signal. This would appear to contradict simple localization arguments which relate an energy-loss interaction distance, d, to the energy-loss E by $d \sim 2\pi E/\hbar v$, for an incident electron velocity v [40]. Prior studies have shown this simple picture is not complete for energy-loss in systems with complicated shapes [41]. Further, the present experiment may be qualitatively different from previous work in this energy-loss region because larger collection angles were used than have been possible before with this energy resolution. Thus we expect these results to be more sensitive to high spatial frequencies. These speculations must be addressed in more detailed experiments.

This preliminary work has shown that a detailed analysis of accurate, high resolution EELS results will yield information about local bonding and electronic structure. The analysis can be made within the constraints of a local picture which may require considerable modification of the conventional band structure due to momentum uncertainty. Therefore, the field emission equipped STEM, which is optimized for high spatial resolution and angle-integrated scattering spectra, is ide-

ally suited for this type of experiment. It is particularly exciting that the defect scattering in the low loss region is very strong relative to the bulk. Thus, EELS may be able to locate single electronic states within structures which have been characterized by high resolution microscopy, to begin the task of relating spatial structure to electronic structure in a fundamental way.

Acknowledgements

We wish to thank S.T. Pantelides for extensive discussion. D. Clarke kindly supplied samples of Si_2N_2O. We wish to thank G.D. Pettit and P.D. Kirchner for preparation of the GaAs heterojunctions used here. K.L. Kavanagh acknowledges support from ONR (L. Cooper) and a Bell Northern Research Fellowship.

References

[1] D.B. Wittry, R.P. Ferrier and V.E. Cosslett, Brit, J. Appl. Phys. 2 (1969) 1967;
M. Isaacson and D. Johnson, Ultramicroscopy 1 (1975) 33.
[2] R.F. Egerton, Ultramicroscopy 3 (1978) 243.
[3] A.J. Craven and T.W. Buggy, Ultramicroscopy 7 (1981) 27;
A.J. Craven, T.W. Buggy and R.P. Ferrier, in: Quantitative Microanalysis with High Spatial Resolution (Arrowsmith, Bristol, 1981) p. 302.
[4] R.F. Egerton, Phil. Mag. 31 (1975) 199.
[5] J.C.H. Spence, Ultramicroscopy 4 (1979) 9.
[6] A.P. Stephens, Ultramicroscopy 5 (1980) 343.
[7] C. Colliex, Ultramicroscopy 18 (1985) 131.
[8] J.C.H. Spence, Ultramicroscopy 18 (1985) 165.
[9] J. Taftø and J. Zhu, Ultramicroscopy 9 (1982) 349;
M.M. Disko, J.C.H. Spence and O.F. Sankey, in: Proc. 42nd Annual EMSA Meeting, Detroit, MI, 1984, Ed. G.W. Bailey (San Francisco Press, 1984) p. 564.
[10] G. Materlik, J.E. Muller and J.W. Wilkins, Phys. Rev. Letters 50 (1983) 267.
[11] G. Hollinger and F.J. Himpsel, Appl. Phys. Letters 44 (1984) 93.
[12] S.T. Pantelides, Phys. Rev. B11 (1985) 2391.
[13] J.J. Ritsko and E.J. Mele, Synthetic Metals 3 (1981) 73.
[14] F.C. Brown and O.P. Rustgi, Phys. Rev. Letters 28 (1972) 497.
[15] P.E. Batson, Rev. Sci. Instr. 57 (1986) 43.
[16] P.E. Batson, in preparation.
[17] C.Y. Wong and P.E. Batson, Appl. Phys. Letters, to be published.
[18] W.Y. Ching and S.Y. Ren, Phys. Rev. B24 (1981) 5788.
[19] S.Y. Ren and W.Y. Ching, Phys. Rev. B23 (1981) 5454.
[20] M. Altarelli and D.L. Dexter, Phys. Rev. Letters 29 (1972) 1100.
[21] P. Durham, J.B. Pendry and C.H. Hodges, Solid State Commun. 38 (1981) 159.
[22] A. Bianconi, Surface Sci. 89 (1979) 41.
[23] S.T. Pantelides and W.A. Harrison, Phys. Rev. B13 (1976) 2667.
[24] W.M. Skiff, R.W. Carpenter and S.H. Lin, J. Appl. Phys., to be published.
[25] R.B.Laughlin, J.D. Joannopoulos and D.J. Chadi, Phys. Rev. B21 (1980) 5733.
[26] R.M. Feenstra and G.S. Oehrlein, Appl. Phys. Letters 47 (1985) 97.
[27] H. Raether, in: Springer Tracts in Modern Physics, Vol. 38, Ed. G. Höhler (Springer, Berlin, 1965) p. 85.
[28] H. Ibach and J.E. Rowe, Phys. Rev. B10 (1974) 710.
[29] J.D. Joannopoulos and M.L. Cohen, Phys. Rev. B7 (1973) 2644.
[30] N.M. Johnson and D.J. Bartelink, in: Physics of SiO_2 and its Interfaces, Ed. S.T. Pantelides (Pergamon, Oxford, 1978) p. 421.
[31] R.B. Laughlin, J.D. Joannopoulos and D.J. Chadi, ref. [30], p. 321.
[32] M.D. Sturge, Phys. Rev. 127 (1962) 768.
[33] H.R. Philipp and H. Ehrenreich, Phys. Rev. 129 (1963) 1550.
[34] R. Gomer, Field Emission and Field Ionization (Harvard University Press, Cambridge, MA, 1961) p. 16.
[35] M. Inokuti, Rev. Mod. Phys. 43 (1971) 297.
[36] P.E. Batson, K.L. Kavanagh, J.M. Woodall and J.W. Mayer, Phys. Rev. Letters 57 (1986) 2729.
[37] J.M. Woodall, G.D. Pettit, T.N. Jackson, C. Lanza, K.L. Kavanagh and J.W. Mayer, Phys. Rev. Letters 51 (1983) 1783.
[38] S.M. Sze, Physics of Semiconductor Devices (Wiley, New York, 1981) p. 849.
[39] J.S. Blakemore, J. Appl. Phys. 53 (1982) R123.
[40] A.J. Craven, J.M. Gibson, A. Howie and D.R. Spalding, Phil. Mag. A38 (1978) 519.
[41] P.E. Batson, Surface Sci. 156 (1985) 720.